Scour around the Circular and Square Profile Piers

Lončar[1], G., Andročec[2], V., Klapčić[3], S., Mišura,[4] I.

[1,3,4]Faculty of Civil Engineering University of Zagreb,
[2]Croatian Academy of Engineering,
goran.loncar@grad.hr, androcec@hatz.hr, sklapcic@student.grad.hr, imisura@student.grad.hr

Abstract: The study shows the methodology and results of the conducted local erosion research around circular and square profile piers under clear-water conditions. Physical and numerical modelling technique has been used to achieve the primary goal for determining the depth of the erosion pit, comparing with the results obtained through the application of empirical equations suggested by a series of authors.

The shape of the pier cross section (circular and square), number of piers in the flow cross section (1, 2, 3) and the flow depth with the corresponding velocity were varied. The granulation of the applied model sediment is uniform and homogeneous (d=2mm). Basic geometrical features of the physical and numerical model were not changed (except for the piers). Based on physical model measurements and numerical model simulations, maximum erosion depths (scour) were determined. The obtained results were compared mutually and with empirical equation results using the same geometric and hydraulic conditions. Numerical simulations were conducted with the aim of Mike 21fm numerical model based on the finite volume method.

The modelling results indicate a more pronounced erosion around the circular piers. The empirical equation of Melville (1997) gives the values of erosion pit depth closest to the measurement results of the physical model and the results of numerical model simulations. The highest degree of resemblance with the models results was achieved in the case where three piers were embedded. The measurement results of the physical model are more consistent with the results of the empirical equation compared to the results obtained by numerical simulations.

Keywords: local scour, pier, numerical model, physical model

1. Introduction

The most common cause of bridge failure is erosion around their piers and abutments. For the purpose of prevention it is necessary to regularly observe the changes of the bedrock. Therefore, the interaction between the water flow and in-water bridge construction elements during the flood condition should be defined as precisely as possible with the aim of preventing bridge damage and consequent loss of life and property. A reduction of the flow cross section due to natural conditions or bridge piers/abutments implementation in the water stream causes a significant disturbance in the flow field. The velocity and the unit discharge increases causing the added erosion of the bedrock. The evolution of the scour pit around the bridge piers and abutments is a dynamic and time-consuming process, but can be significantly accelerated in a relatively short time during the occurrence of flood waves.

Since 1950 in the United States, 60% of 823 bridges have been partially damaged or destroyed as a result of intensive scouring (Shirola and Holt, 1991). The USA Federal Highway Association has reported that every year about 50 bridges fail in the USA. Brice and Blodgett (1978) state that 50% of the bridge failures in the USA are caused by local erosion. Miller (2003) reported that the breakdowns of bridges in New York and Tennessee resulted in a loss of 18 lives during the period 1987 – 1989. Also seven people were killed because of the bridge failure over the river Arrayo Pasajero in 1995. According to Richardson and Davis (2001), storm Alberto in Georgia was responsible for 130 million dollar damage needed for reparatory and reconstruction of more than 100 bridges. Many bridges were broken or damaged during major floods in Turkey (Yanmaz, 2002). In the United States, the state of river bridges has been continuously monitored since 1991, and it was found that 17,000 were in a critical condition due to local erosion problems (Lagasse et al., 1998). The biggest bridge in Croatia that has failure due to the scouring is "Jakuševac" bridge on the railway Velika Gorica - Sesvete, at the point of bridging the Sava River near Mičevac. The bridge was built in 1968. On March 30, 2009, at 22:30, the stability of the load-bearing structure collapsed during the passage of a freight train.

The stability of the watercourse depends on the sediment transport regime. Riverbed instability is a natural phenomenon resulting from the erosion and sedimentation process that develops gradually at medium flow conditions or evolve rapidly during the flooding regime (Melville and Coleman, 2000). Local erosion is usually divided into: a) clear-water erosion and b) live bed erosion. Therefore, the local erosion equations are categorized in this way.

Clear-water erosion (scour) occurs in case of no sediment removal upstream of the bridge. The degree of erosion depends on the local flow field defined by the cross sectional geometry. Erosion around the bridge piers develops relatively fast in the initial stage under clear-water conditions, and due to an increase in the erosion pit, it reduces stresses and achieves balance and interrupts further development of the erosion pit.

Live bed erosion occurs in the presence of sediment transport upstream from the bridge. This kind of erosion refers to the case of intense erosion pit development in the initial stage, followed by the reduced scouring until the achievement of the equilibrium conditions (sedimentation and erosion of the material in the erosion pit area is equal).

The measurements of the maximum depth of the erosion pit under clear-water condition were initially performed on the physical model. Variations in geometric and hydraulic characteristics are given in table 1 (18 experiments). Thereafter, a numerical model of sediment transport was implemented for the same conditions that were used in the previously performed analyses on the physical model.

The following parameters and conditions were used in the course of the investigation:
- the width of the experimental channel (distance of lateral vertical walls $B = 0.8$ m, constant in all experiments);
- diameter of the uniform model sediment ($d = 0.002$ m $= 2$ mm);
- piers cross section and diameter (circular $D = 0.1$ m, square $D = 0.1$ m);
- pier configuration along the contraction profile (with 1/2/3 piers);
- inflow depth ($h = 0.04$; 0.05 ; 0.06 m);
- inflow average flow velocity ($v = 0.22$; 0.26 ; 0.29 m/s);
- experiment duration on the physical and numerical model (14,400 s);
- model discharge $Q = 0.011$ m³/s.

2. Physical model

The physical model was created in the Hidrotehnic Laboratory of the Faculty of Civil Engineering, University of Zagreb (Figures 1 and 2). The physical model is 2.0 m long and 0.8 m wide. It consists of inflow part where a uniform flow develops, working section with quartz sand of 2 mm diameter where piers are embedded, and outlet zone in which the water depth is regulated. The discharge regulation valve is located on the model entrance and Thomson measurement overflow on the

Fig. 1 – Physical model for local erosion analysis around the pier

model exit section. The needle probes are used to measure water level and erosion pit depth.
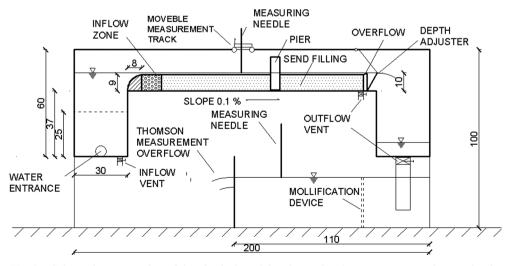

Fig. 2 – Schematic presentation of the physical model and associated measurement equipment for the local erosion analysis around the pier

Table 1 – Nomenclature of experiments on physical and numerical model with basic geometric and hydraulic characteristics (N – number of piers in flow profile, KR – circular cross section, KV – square cross section, a – the transversal width of the gap between the outer edges of the piers, $h_{X=1.0}$ – water depth before pier section at the chainage $x = 1.0$ m, $h_{X=1.7}$ – water depth after pier section at the chainage $x = 1.7$ m, V – average flow velocity before pier section at the chainage $x = 1.0$ m)

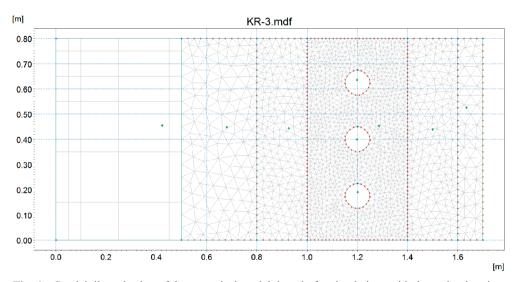| Exp. num.	N	form	a / D (1)	$h_{X=1.0\,m}$ (m)	$h_{X=1.7\,m}$ (m)	V (m/s)
1	1	KR		0.063	0.062	0.22
2	1	KR		0.053	0.05	0.26
3	1	KR		0.048	0.042	0.29
4	2	KR	2	0.063	0.062	0.22
5	2	KR	2	0.053	0.05	0.26
6	2	KR	2	0.049	0.042	0.29
7	3	KR	1.25	0.064	0.062	0.22
8	3	KR	1.25	0.054	0.05	0.26
9	3	KR	1.25	0.05	0.042	0.28
10	1	KV		0.063	0.062	0.22
11	1	KV		0.053	0.05	0.26
12	1	KV		0.048	0.042	0.29
13	2	KV	2	0.063	0.062	0.22
14	2	KV	2	0.053	0.05	0.26
15	2	KV	2	0.049	0.042	0.29
16	3	KV	1.25	0.066	0.062	0.21
17	3	KV	1.25	0.056	0.05	0.25
18	3	KV	1.25	0.052	0.042	0.27

3. Numerical model

The numerical model Mike 21fm (www.dhigroup.com) was used. The model solved 2D Navier-Stokes equations for noncompressible fluid using Reynolds's averaging and Boussinesq hydrostatic assumption. For spatial discretisation, the final volume method with continuous and non-overlapping cells was used. The model spatial domain (Figure 3) was discretised in the horizontal direction with structured rectangular mesh at the inflow part of the model (square cells with area $2.5*10^{-3}$ m^2) and unstructured triangular mash elsewhere (triangular cells with average area $1.8*10^{-3}$ m^2 ; $6.0*10^{-4}$ m^2 ; $2.0*10^{-4}$ m^2).

The bottom was adopted as initially horizontal with a constant depth of 0.5 m in the area covered with square cells and with a constant depth of 0.05 m on the remaining part of the model domain (identical to the actual dimensions of the physical model). Along the lateral vertical walls a zero flow velocity condition was imposed (no-flow boundary).

At the left open boundary (the boundary condition of the hydrodynamic part of the model) constant inflow discharge Q = 0.011 m³/s was used (see Table 1). On the right open boundary constant water surface levels were used, aiming identical water depth at chainage x = 1.7 m as measured on the physical model under the same hydraulic condition (column $h_{X=1.7m}$, see Table 1). The initial conditions for flow velocity components were adopted with 0 m/s in two horizontal directions for all numeric cells. Numerical simulations covered the period of 14,400 s (4 hours).

The closure of the turbulence model relies on Smagorinsky concept (1993), using Smagorinsky coefficient with spatial uniform value 0.2. Roughness was parameterised using Manning coefficient with spatial uniform value 0.015 m$^{1/3}$/s.

Fig. 4 – Spatial discretisation of the numerical model domain for simulations with three circular piers and diameter of 0.1 m

The integral formulation of continuity and momentum equations for 2D shallow water in the Cartesian coordinate system reads (Sleigh and Gaskel, 1998; Zhao et al., 1998):

$$\frac{\partial \boldsymbol{U}}{\partial t} + \nabla \cdot \mathrm{F}(\mathrm{U}) = \mathrm{S}(\mathrm{U}) \tag{1}$$

$$U = \begin{bmatrix} h \\ hu \\ hv \end{bmatrix} \quad F_x = \begin{bmatrix} hu \\ hu^2 + gh/2 \\ huv \end{bmatrix} \quad F_y = \begin{bmatrix} hv \\ hvu \\ hu^2 + gh/2 \end{bmatrix} \quad S = \begin{bmatrix} hs \\ gh(S_{0x} - S_{fx}) \\ gh(S_{0y} - S_{fy}) \end{bmatrix} \quad \text{(2a,b,c,d)}$$

$$S_{fx} = \frac{n^2 u \sqrt{u^2 + v^2}}{h^{4/3}} \qquad S_{fy} = \frac{n^2 v \sqrt{u^2 + v^2}}{h^{4/3}} \tag{3}$$

where: U conservative variable vector; F flux vector function; S source/sink vector; S_{0x} and S_{0y} bottom slope in x and y direction; S_{fx} and S_{fy} energy line slope defined with Manning equation, n Manning coefficient.

Using the Green-Gauss theorem in integration of equation 1 along i-th cell gives:

$$\int_{Ai} \frac{\partial U}{\partial t} d\Omega + \int_{Ai} S(U) d\Omega = -\int_{\Gamma i} (F \cdot n) dS \tag{4}$$

where: A_i i-th cell area, Ω integration variable defined on A_i, Γ_i wetted perimeter of cell A_i, ds integration variable along wetted perimeter, n vector of outer normal. Horizontal convective members are calculated using Riemann solver with Roe approximation (Roe, 1981; Alcrudo and Garcia-Navarro, 1993; Toro, 1997).

The sediment transport model uses the following set of equations for transport intensity calculation:

$$\Phi_t = \frac{C^2}{2g} \theta^{2.5} \tag{5}$$

$$\Phi_t = \frac{q_t}{\sqrt{(s-1)gd^3}} \tag{6}$$

$$\theta = \frac{U_f^2}{(s-1)gd} \tag{7}$$

where: C Chezy coefficient, q_t total mass flux of sediment, g gravity constant, θ nondimensional bed stress, U_f shear velocity, d grain diameter (adopted $d = 2$ mm); s relative sediment density (adopted 2.65).

The above formulation assumes that nondimensional bottom stress is much larger than the critical Shields parameter for erosion initiation. At the left inflow open boundary of the sediment transport model zero sediment flux condition was used, while on the outflow open boundary zero gradient flux for sediment was used.

4. Empirical equations

The previous research shows that local erosion around bridge piers depends on the bottom material properties (primarily granulation), watercourse configuration, flow characteristics, fluid properties and bridge pier geometry. Most of the parameters are in mutual interaction. For the purposes of estimation of erosion pit depth in clear-water condition ($V / V_c < 1$, V_c critical flow velocity for erosion initiation), empirical equations according to the following authors were extensively used:

$$d_s = 1.4\, D \qquad\qquad\qquad \text{Breusers (1965)} \qquad (8)$$

$$d_s = 2.42\, D \left(\frac{2V}{V_c} - 1\right)\left(\frac{V_c^2}{g \cdot D}\right)^{1/3} \qquad \text{Hancu (1971)} \qquad (9)$$

$$d_s = 1.84\, D \left(\frac{h}{D}\right)^{0,3} \qquad\qquad \text{Jain (1981)} \qquad (10)$$

$$d_s = 0.46\, K_s\, D \left(\frac{h}{D}\right)^{0,4}\left(\frac{h}{d}\right)^{0,07} h^{-0,32} \quad \text{Gao (1993)} \qquad (11)$$

$$d_s = K_{yb}\, K_D\, K_s \qquad\qquad\qquad \text{Melville (1997)} \qquad (12)$$

$$d_s = 0.24 \left(\frac{0,8 \cdot h \cdot V}{\sqrt{d}}\right)^{1/3} - h \qquad \text{Antunes do Carmo (2005)} \quad (13)$$

where: $V_c = 0.0305\, d^{0.5} - 0.0065\, d^{-1}$ for 1mm $< d_{50} <$ 100mm (Melville i Coleman, 2000), K_{yb} coefficient for the influence of pier foundation size ($K_{yb} = 2.4\, D$ for $D / d < 0.7$; $K_{yb} = 2\,(dD)^{0.5}$ for $0.7 < D / d < 5$; $K_{yb} = 4.5\, D$ for $D / d > 5$; Melville i Coleman, 2000), K_D pier – sediment relation coefficient factor ($K_D = 0.57$ log (2.24 D/d) for $D / d < 25$; $K_D = 1$ for $D / d > 25$; Melville and Sutherland, 1988), K_S coefficient for the shape of pier cross section ($K_S = 1$ for circular ; $K_S = 1.22$ for square pier).

The effect of pier group depends primarily on the distance between the piers and piers layout within the watercourse. If the flow direction is orthogonal to the piers line ($\alpha = 90\,°$) and a/D > 7, all the piers forming the group act as a single pier (separated erosion pits around every individual pier). On the other hand, if a/D < 0.5, one common pit around the pier group will be formed (Salim and Jones, 1999).

5. Measurement and modelling results

Figure 5 shows measured (physical model) and calculated (numerical model) depths of erosion pit for experiment conditions 1-18 (Table 1).
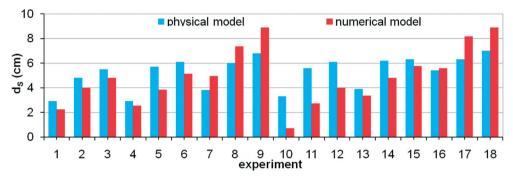

Fig. 5 – Measured (physical model) and calculated (numerical model) depths of erosion pit in experiment conditions 1-18 (table 1)

According to the numerical model results, the average depth of the erosion pit for the circular pier/piers is 2% higher than in the case with the square pier/piers. The measurement results of the physical model show that the depth of the erosion pit for the square pier/piers was on average higher by 15% than for the circular pier/piers. Furthermore, the layout with two circular piers causes an increase in the depth of the erosion pit by an average of 8% (physical and numerical model), while the layout with 3 circular piers results in a higher depth of the erosion pit by an average of 63% (physical and numerical model). When one increases the number of piers, the increase of erosion pit depth is more pronounced. Embedding of two squared piers results with increase of erosion pit depth by 85%, while in the case of three embedded piers the increase of erosion pit depth is almost 3 times (285%). These percentages represent mean values of all measurement results and numerical simulations. The average measured erosion depth in all 18 experiments is 33% higher than the average value obtained by using the numerical model.

Figures 6 and 7 show vertically averaged flow fields obtained by the numerical model for the corresponding conditions shown in Table 1. Figures 8 and 9 show appertaining calculated erosion fields in the model spatial domain.

Figure 10 shows the comparison of the erosion pit depths computed by numerical model and calculated on the basis of the empirical equations 8 – 13. Figure 11 shows the local erosion around two circular and square piers after achieving the equilibrium condition in experiments 6 and 15 on the physical model.
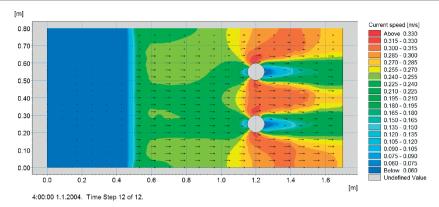
Fig. 6 – Vertically averaged flow field for two circular piers of a diameter D = 0.1 m with a water depth $h_{(X = 1.7m)}$ = 0.06 m used for the outflow open boundary condition
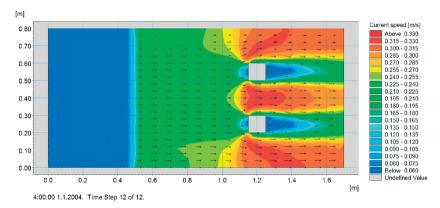

Fig. 7 – Vertically averaged flow field for two square piers of a diameter D = 0.1 m with a water depth $h_{(X = 1.7m)}$ = 0.06 m used for the outflow open boundary condition
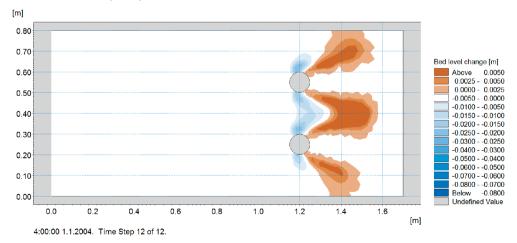

Fig. 8 – Erosion/sedimentation field for two circular piers of a diameter D = 0.1 m with a water depth $h_{(X = 1.7m)}$ = 0.06 m used for the outflow open boundary condition
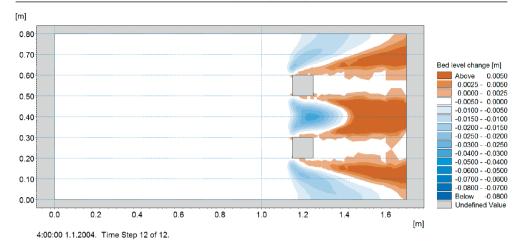
4:00:00 1.1.2004. Time Step 12 of 12.

Fig. 9 – Erosion/sedimentation field for two square piers of a diameter D = 0.1 m with a water depth $h_{(X=1.7m)}$ = 0.06 m used for the outflow open boundary condition
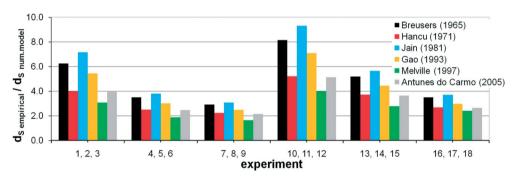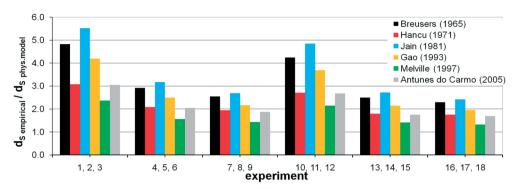

Fig. 10 – Comparison of the erosion pit depths computed by the numerical model and calculated on the basis of empirical equations 8 – 13

Fig. 11 – Local erosion around two circular and square piers after achieving the equilibrium condition in experiments 6 and 15 on the physical model (see Table 1)

Figure 12 shows the comparison of the erosion pit depths measured on the physical model and calculated on the basis of empirical equations 8 – 13.

Fig. 12 – Comparison of the erosion pit depths measured on the physical model and calculated on the basis of empirical equations 8 – 13

The results in Fig. 10 indicate that closest results of the erosion pit depth computed by the numerical model and obtained using the empirical equation given by Melville (1997) is in the presence of three piers. On the other hand, in the case of a single pier, the numerical model gives significantly lower values (on average five times lower). Recognizing the absence of the member in the empirical equation that directly represents the influence of the pier group, it can be concluded that the contribution of the pier group is indirectly imposed in the empirical equation.

The results given in Fig. 12 point out that the measurement results of the physical model, the same as the results obtained by numerical simulations, best correspond to the results of Melville (1997) empirical equation. It should be noted that the highest degree of resemblance between the measured and empirical values was achieved in the case of the layout with three piers. In the layout with one pier, the measurement of the physical model gives significantly lower values of erosion depths than the empirical equations (twice lower in the case of square pier and empirical equation according to Melville (1997)). Therefore, it could be concluded that the empirical equations contain an additional security coefficient that covers the stochastic nature of the erosion process in realistic environmental conditions.

6. Conclusion

A study of local erosion around pier/piers of circular and square profiles in clear-water conditions was carried out. The technique of physical and numerical modelling

was applied and the depth of the erosion pit was measured and calculated. The measurement results of the physical model and obtained by numerical simulations were compared with the results of empirical equations given by a series of authors. In the scope of investigation some geometric and hydraulic parameters were varied: the shape of the pier cross section (circular and square), the number of piers in the partition profile (1, 2, 3), and the flow depth and flow velocity. The granulation of the applied model sediment is uniform and homogeneous (d = 2 mm).

The measurement results of the physical model and the implementation of numerical model simulations point to a more pronounced erosion around the pier/piers of circular cross section relative to the pier/piers of square cross section. Thus the depth of the erosion pit in the case of circular pier/piers is higher by an average of 5% (for 1, 2 and 3 piers on the physical and numerical model).

It is noted that Melville's (1997) empirical equation takes into account the greatest number of hydraulic and geometric properties of the watercourse and the piers themselves, and that the result of its application is closest to the measurement results of the physical model or the results of numerical simulations. The highest degree of similarity with model results was achieved in the presence of three piers, when the Melville empirical equation (1997) gives only 15% greater depth of the erosion pit than measured on the physical model.

The measurement results of the physical model are more consistent with the results of empirical equation compared to the results obtained by numerical simulations.

The future research should be focused on field work with measurement campaigns undertaken immediately after the occurrence of extreme flooding conditions.

References

Alcrudo, F., Garcia-Navarro, P. (1993): A high resolution Godunov type scheme in finite volumes for the 2D shallow-water equation, *Int. J. Numer. Methods Fluids*, 16(6), pp. 489-505.

Antunes do Carmo, J.S. (2005): Experimental study on local scour around bridge piers in rivers*, WIT Transactions on Ecology and Environment*, Vol. 83, IMAR – University of Coimbra, Deprtment of Civil Engineering, Portugal, pp. 3 - 13.

Breusers, H.N.C. (1965): *Scour around drilling platforms,* Bulletin, Hydraulic Research 1964 and 1965, I.A.H.R., Vol. 19.

Brice, J.C., Blodgett, J.C. (1978): *Countermesures for hydrulic problems at bridges*, Vols. 1 and 2., Federal highway administration, U.S Department of Transportation , Washington D.C., USA.

Gao, D., Posada, G.L., Nordin, C.F. (1993): *Pier scour equations used in the Peoples Republic of China – Review and Summary,* Proc., A.S.C.E. National Hydraulics Conference, San Francisco, California, U.S.A., pp. 1031-1036.

Hancu, S. (1971): *Sur le calcul des affouillements locaux dams la zone des piles des ponts,* Proc., 14. I.A.H.R. Congress, Paris, France, Vol.3, pp. 299-313.

Jain, S.C. (1981): Maximum clear – water scour around cylindrical piers*, Journal of Hydraulics Engineering*, A.S.C.E., 107(5), pp. 611-625.

Lagasse, P.F., Schumm, S.A., Zevenbergen, L.W. (1998): *Quantitative techniques for stream stability analysis,* Proc., 27. Congress of the International Association for Hydraulic Research, San Francisco, California, U.S.A., August, pp. A147-A153.

Melville, B.W. (1997): Pier and abutment scour – An integrated approach*, Journal of Hydraulic Engineering*, A.S.C.E., 123(2), pp. 125-136.

Melville, B.W., Coleman, S.E. (2000): *Bridge scour*, Water Resources Publications, LLC, 550 pp.

Richardson, J.R., Davis, P.M. (2000): *Practical method for calculating contraction scour*, Proc. A.C.S.E. national Hydraulics Conference, Buffalo, New York, USA, pp. 6-10.

Roe, P., L. (1981): Approximate Riemann solvers, parameters vectors and difference schemes, *Journal of Computationals Physics*, 43, pp. 357-372.

Shirhole, A.M., Holt, R.C. (1991): Planning for a comprehensive bridge safety program, Transportation research record 1290, Vol. 1, Transportation Research Board, National Research Council, Washington, D.C., U.S.A., pp. 39-50.

Sleigh, D. H., Gaskel, P. H. (1998): An unstructured finite volume algorithm for predicting flow in rivers and estuaries, *Computer and Fluids*, 27(4), pp. 479-508.

Smagorinsky, J. (1993): Some historical remarks on the use of nonlinear viscosities, In: *Large eddy simulations of complex engineering and geophysical flows* (B. Galperin and S. Orszag Eds.), Cambridge Univ. Press, pp. 1-34.

Toro, E., F. (1997): *Riemann Solvers and Numerical Methods for Fluid Dynamics*, Springer, Germany.

Yanmaz, A. M. (2002): *Kopru Hidroligi*, ODTU Gelistirme Vakfı Yayıncılık ve Iletisim A.S. Yayınları, METU Press, ISBN 975-7064-55-6.

Zhao, D. H., Shen, H.W., Tabios, G.Q., Tan, W.Y. (1994): Finite-volume two dimensional unsteady flow model for river basins, *Journal of. Hydraulic Engineering*, ASCE, 120(7), pp. 833-863.